# CFD-simulations of a Piston Accumulator using STAR-CCM+

Vebjørn Nicholas Brevik

Bachelor's thesis in Marine Technology
Bergen, Norway 2019

Høgskulen på Vestlandet

Western Norway
University of
Applied Sciences

# CFD-simulations of a Piston Accumulator using STAR-CCM+

Vebjørn Nicholas Brevik

Department of Mechanical- and Marine Engineering
Western Norway University of Applied Sciences
NO-5063 Bergen, Norway

IMM 2019-M38

Western Norway University of Applied Sciences
Faculty of Engineering and Science
Department of Mechanical- and Marine Engineering
Inndalsveien 28,
NO-5063 Bergen, Norway



| | |
|---|---|
| *Norsk tittel:* | CFD-simuleringer av en stempelakkumulator ved hjelp av STAR-CCM+ |

Author, student number: Vebjørn Nicholas Brevik, 182784

| | |
|---|---|
| Study program: | Marine Technology |
| Date: | June 2019 |
| Report number: | IMM 2019-M38 |
| Supervisor at HiB: | Boris V. Balakin |
| Assigned by: | Boris V. Balakin in cooperation with OneSubsea AS |
| Contact person: | Gleb Pisarev |
| Antall filer levert digitalt: | 1 |

## Preface

This thesis is submitted as a final assignment for obtaining the degree of Bachelor of Science in Marine Technology at the Department of Mechanical and Marine Engineering at the Western Norway University of Applied Sciences (WNUAS). The thesis was conducted in the spring 2019 and lasted from January to May.

I would like to thank my supervisor Prof. Boris V. Balakin from the Department of Mechanical and Marine Engineering for his support throughout the project. His knowledge and expertise in computational fluid dynamics, STAR-CCM+ and hydraulics was essential for completing this thesis. I also want to thank Prof. Gleb Pisarev and OneSubsea AS for providing me with technical data and information for the project, and for giving me the opportunity to work with a real problem.

Last but not least I want to express my gratitude towards Otto Andreas Moe for letting me base my model on his work, and for providing me with dimensions, useful information and support.

Vebjørn N. Brevik

# Abstract

This thesis is construced to study the physical behaviour of a 10-l hydraulic piston accumulator during discharge under different precharge conditions to gain a better understanding of the odd pressure behaviour measured by OneSubsea. The accumulator is a part of the network of a hydraulic power unit (HPU) installed on a platform, and the system is connected to a subsea multiphase pump with a hydraulic umbilical. When discharging starts the pressure experiences a rapid pressure reduction, and OneSubsea is interested in understanding the details of this behaviour.

The problem is approached by creating a reduced model of the accumulator in the computational fluid dynamics (CFD) software STAR-CCM+. After creating a stable model, simulations at five different precharge pressures were conducted. For each case the pressure, temperature, velocity and volume flow were monitored. The results of these simulations are analyzed and compared by studying the graphs and their slopes. The aim of this thesis is to create a realistic model for the hydraulic accumulator which can be used for the development of a numerical model for a software-based detection of leaks.

Based on the results, the precharge pressure is clearly affecting the discharge time. At the lowest precharge pressure the accumulator discharges in 42 s, compared to 20 s for the highest precharge pressure condition. This is expected because of the reduced amount of barrier fluid in the accumulator at higher precharge pressures. Based on the graphs, the pressure reduction is smoother at higher precharge pressures. This is due to the increased amount of nitrogen in the accumulator increasing the driving force, resulting in a more stable piston movement.

The volume flow starts at approximately 50 l/h and drops to 25 l/h in all simulations. This is a large deviation from the measured average volume flow of 0.5 l/h, and this leads to a faster discharge time in the model. For the lowest precharge pressure simulated at 40 bara, which is the same value for the measured accumulator discharge, the discharge time is 42 s compared to 156 s for the actual accumulator. The results from this thesis should therefore be assessed with caution.

# Sammendrag

Denne oppgaven er laget for å studere den fysiske oppførselen til en 10-l hydraulisk stempelakkumulator under utladning ved forskjellige ladningstrykk for å oppnå en bedre forståelse av den merkelige trykkoppførselen målt av OneSubsea. Akkumulatoren er en del av kretsen til en hydraulisk kraftenhet (HPU) installert på en platform, og systemet er koblet til en undervanns flerfasepumpe ved en hydraulisk navlestreng (umbilical). Når utladningen starter så faller trykket hurtig, og OneSubsea er interessert i å forstå detaljene rundt denne oppførselen.

Oppgaven er tilnærmet ved å lage en redusert model av akkumulatoren i numerisk-fluiddynamikk-verktøyet STAR-CCM+. Etter å ha laget en stabil model, ble simuleringer utført ved fem forskjellige ladningstrykk. For hver simulering så ble trykket, temperaturen, hastigheten og volumstrømmen overvåket. Resultatet fra disse simuleringene blir analysert og sammenlignet ved å studere grafene og stigningstallene deres. Målet ved oppgaven er å lage en realistisk modell for akkumulatoren som kan bli brukt til å utvikle en numerisk modell for programvare-basert oppdagelse av lekkasjer.

Fra resultatene så er det tydelig at endring av forladningstrykket påvirker utladningstiden. Ved det laveste forladningstrykket så er utladningstiden 42 s, sammenlignet med 20 s ved det høyeste forladningstrykket. Dette er forventet siden væskenivået i akkumulatoren er lavere ved høyere forladningstrykk. Fra grafene så er det tydelig at trykkreduksjonen er mer stabil ved høyere forladningstrykk. Dette er på grunn av den økte mengden av nitrogen i akkumulatoren. Dette øker drivekraften, som resulterer i en mer stabil stempelbevegelse.

Volumstrømmen starter ved omtrent 50 l/t og faller til 25 l/t i samtlige simuleringer. Dette er et stort avvik fra den målte gjennomsnittsverdien på 0.5 l/t fra det ekte systemet, og dette fører til en hurtigere utladningstid for modellen. For det laveste ladningstrykket simulert ved 40 bara, som har det samme ladningstrykket som den ekte akkumulatoren, så er utladningstiden 42 s sammenlignet med 156 s for den ekte akkumulatoren. På grunn av dette så burde resultatene fra denne oppgaven vurderes med forsiktighet.

# Table of Contents

# List of Figures



# List of Tables

# 1. Introduction

Leakages in pipelines are undesirable incidents due to cracks or holes in the material. This leads to considerable amounts of oil and gas losses from the installations, and this presents a risk to the environment. From the economical point of view, leakages costs oil and gas operators a large amount of financial loss. It might also reduce the efficiency of equipment, for instance the power capacity of an accumulator. Operators spend time and financial effort on detecting, localizing and fixing leakages. Therefore, it has been development of different systems for efficient and precise detection and localization of leakages in pipelines over the last decades.

Several leak detection (and localization) systems (LDS) has been developed to make it possible to monitor the flow in pipelines. These are divided into two groups; external and internal based LDS. For external solutions local leak sensors generate a leak alarm which can be evaluated. They are often charactherized by a good sensitity to leaks and accuracy related to leak localization. However, system costs and complexity of installation limits these applications to high-risk areas, such as near rivers or nature protection areas. An example of external LDS are acoustic emission detectors, where escaping liquids creates an acoustic signal as it passes through a crack in the pipe. Internal LDS utilize field sensors (e.g. for flow, pressure and temperature) for monitoring. The field signals are used for assuming a leak. An example for internal LDS is pressure/flow monitoring. This method is based on the fact that sudden leaks results in sudden changes of pressure and flow at inlet and outlet, respectively. [1]

By creating a realistic CFD-model (Computational Fluid Dynamics) of the hydraulic accumulator, it can be used for designing systems where hydraulic accumulators are present. Based on the pressure-flow deviation method, the calculated pressure and flows from the model should be equal to the measured values if there is no leak in the pipeline. Leaks can be determined if there are deviations between measured values and calculated values. The measured outlet pressure and flow is applied as boundary conditions in the model. The calculated values are usually not equal to the measured values, even if there is no leak in the pipeline. This is a result of the inaccuracies in measured values and the parameters used in the model, such as density of barrier fluid, roughness, diameter of the pipe wall and unsteady friction. For this reason, a tuning process needs to be conducted in a pipeline assuming no leaks. When the deviation between the model and measurements exceeds a minimum value, a process of sizing and locating the leak is initialized. [2]

The Western Norway University of Applied Sciences (WNUAS) in collaboration with OneSubsea are after the development of a numerical model for the software-based detection of leaks. This code is supposed to predict leaks «on the go» based on own analysis on the measurements from the control system. According to measurements from OneSubsea's control system, the pressure during accumulator discharge displays an odd behaviour. Upon discharge, there is a rapid pressure drop before it stabilizes and assumes normal consumption. The pressure behaviour is not clearly understood, and OneSubsea is interested in understanding every detail of the behaviour upon discharge when used for leak compensation. For this reason, this thesis is constructed to create and analyze a model using the CFD-software STAR-CCM+. The model is used to gain a detailed description of the physical behaviour of the accumulator during discharge.

In Table 1 the dimensions of the actual accumulator, piston and technical data for the pipeline is listed. It is based on the geometry of a 10-litre piston accumulator used in OneSubsea's installed HPU (hydraulic power unit) on a platform. The model is reduced to 15 degrees of the actual geometry to save computational effort. Symmetry conditions are applied to make the reduced model represent the complete geometry. The accumulator is connected to a pipeline from which it provides barrier fluid to subsea installations approximately 10 kilometres from the platform. The barrier fluid used is Morlina S2 BL 5, which is a low viscosity, solvent refined mineral oil blended with zinc free additives.

| **Dimensions of Accumulator** | |
|---|---|
| Accumulator Inner Length | 0.693 m |
| Accumulator Inner Diameter | 0.140 m |
| Fluid Port Inner Diameter | 0.019 m |
| **Dimensions of Piston** | |
| Outer Height | 0.08 m |
| Inner Height | 0.06 m |
| Outer Diameter | 0.14 m |
| Inner Diameter | 0.1044 m |
| Piston Volume | 0.000718 $m^3$ |
| Piston Mass | 5.779 kg |
| Virtual Piston Height | 0.0466 m |
| Precharge Placement of Piston | 0.6464 m |
| **Dimensions of Pipeline** | |
| Tubing on Platform Length | 80 m |
| Tubing on Platform Internal Diameter | 0.014 m |
| Coupling Upstream Umbilical | 5/8'' |
| Umbilical from Platform to Seabed | 209 m |
| Umbilical from Platform to Seabed Internal Diameter | 0.0159 m |
| Umbilical on Seabed Length | 9474 m |
| Umbilical on Seabed Internal Diameter | 0.0159 m |

Table 1-1: Dimensions of the accumulator, piston and pipeline
(with permission from Otto Andreas Moe)

# 2. Theoretical Background

Before starting the CFD-analysis of the problem, it is important to determine the numerical values and expressions for the initial conditions and boundary conditions. In this section the theoritical background for the calculations is stated. The initial values and expressions that needs to be determined is

- The initial conditions of the nitrogen gas
- An expression for the outlet pressure

First it is neccessary to review some of the physics of accumulators.

## 2.1 Piston Accumulator

For a piston accumulator, the physical values of the nitrogen gas are evaluated at three conditions. The precharge condition is the condition of the gas before the accumulator is installed in the hydraulic system, and the piston is all the way down. The pressure, temperature and volume at precharge condition is represented by $P_0$, $T_0$ and $V_0$, respectively.

When the accumulator is installed and the fluid pressure becomes greater than $P_0$, the fluid pressure will compress the gas and cause the piston to move away from the fluid port opening. This is called charging the accumulator. The pressure, temperature and volume when the accumulator is fully charged is denoted by $P_1$, $T_1$ and $V_1$, respectively.

During discharge, the fluid pressure drops, and the gas pressure starts pushing the piston downwards. When the accumulator is fully discharged, the pressure, temperature and volume is defined by $P_2$, $T_2$ and $V_2$, respectively. [3]

### 2.1.1 Piston Friction

The piston moving inside the accumulator will experience a friction force when sliding against the wall. The direction of the friction will depend on the piston movement and is always working in the opposite direction of the movement. This friction force divided by the wall area exposed to fricton represents the difference in pressure between the gas and fluid side of the piston. Therefore, the gas pressure, $P_{gas}$, during charging is

$$P_{gas} = P_{fluid} - F_f / A_w \tag{2.1.1}$$

where $P_{fluid}$ is the pressure of the fluid, $F_f$ is the friction force and $A_w$ is the exposed wall area. During discharge, the friction force will work in the opposite direction, and the pressure of the gas is

$$P_{gas} = P_{fluid} + F_f / A_w \tag{2.1.2}$$

From this, the initial pressure of the nitrogen gas is calculated. It should be noted that the friction force is considered constant. [4]

## 2.2 Initial Conditions of Nitrogen Gas

After determining the initial gas pressure in the previous section, theoretical calculations need to be made to aquire:

- the initial temperature of the gas
- the initial placement of the piston

To determine the initial conditions of the gas, the nitrogen gas needs to be considered as an ideal gas. Then the mass of the gas, $m$, is determined from the ideal gas equation,

$$m = PV/RT \tag{2.2.1}$$

where $R$ is the individual gas constant for nitrogen, and $P$, $V$ and $T$ is the pressure, volume and temperature of the gas, respectively. The mass of the gas will be constant throughout the entire cycle, based on the conservation of mass principle. When the accumulator charges for the first time, it initially has no fluid inside and the piston is all the way down. The charging is rapid, and therefore it is considered an adiabatic compression. Following this assumption, the following equation may be utilized to determine the volume after the compression:

$$PV^{\gamma} = Constant \tag{2.2.2}$$

Here $\gamma$ is the adiabatic constant, which is 1.4 for a diatomic gas. Moving on, the accumulator is discharged down to the minimum working pressure. During this process, heat is exchanged to the environment. However, if this process is slow enough, it is sometimes considered isothermal. The following equation holds:

$$PV^{n} = Constant \tag{2.2.3}$$

Here $n$ is the polytropic constant, which is set as 1.0 for an isothermal process. After another adiabatic compression, using formula 2.2.2, the initial condition of the gas is reached. By changing equation 2.2.1, the initial temperature is given by

$$T = PV/mR \tag{2.2.4}$$

The initial volume of the nitrogen was determined by equation 2.2.2. The volume of the nitrogen gas is given by

$$V = A_{top}h \tag{2.2.5}$$

where $A_{top}$ is the top area of the piston and $h$ is the initial placement of the piston. By changing equation 2.2.5, the initial placement of the piston is given by

$$h = V/A_{top} \tag{2.2.6}$$

The initial conditions of the gas have now been determined. [3]

## 2.3 Pressure at Outlet

At the bottom of the model, it is necessary to have a pressure outlet. A field function is needed to determine the pressure at the outlet. According to the Bernoulli equation for incompressible, steady flow along a streamline in inviscid regions of flow,

$$\frac{P}{\rho} + \frac{v^2}{2} + gz = constant \tag{2.3.1}$$

where $\rho$ is the density, $v$ is the velocity, $g$ is the gravitational constant and $z$ is the elevation of the fluid. The Bernoulli equation can also be written between any two points on the same streamline as

$$\frac{P_1}{\rho} + \frac{v_1^2}{2} + gz_1 = \frac{P_2}{\rho} + \frac{v_2^2}{2} + gz_2 \tag{2.3.2}$$

Equation 2.3.1 and 2.3.2 does not account for the viscous effects (friction from pipe) and the effect of different components that disturbs the streamlined structure of flow (pumps, turbines, entries, exits, fittings, valves etc…). In this project, it will be necessary to find the pressure loss due to friction, a ball

valve and a pipe exit to a large tank (local resistance of large volume type). A deviation of the Bernoulli equation, using energy equations and including the kinetic energy correction factors, provides the following equation for steady, incompressible flow:

$$\frac{P_1}{\rho g}+\alpha_1\frac{v_1^2}{2g}+z_1+h_{pump,u}=\frac{P_2}{\rho g}+\alpha_2\frac{v_2^2}{2g}+z_2+h_{turbine,e}+h_{L,total} \tag{2.3.3}$$

where $\alpha_1$ and $\alpha_2$ is the kinetic energy correction factor for the flow at point 1 and 2, respectively, $h_{pump,u}$ is the useful head delivered to the fluid by the pump, $h_{turbine,e}$ is the extracted head removed from the fluid by the turbine and $h_{L,total}$ is the irreversible head loss between point 1 and 2 due to all components of the piping system other than the pump or turbine. In this project, the pump and turbine contributions are not relevant because there are none located between the accumulator (point 1) and the manometer (point 2), and the pump is closed of from the circuit during discharge. But the other components will be represented by the total head loss, $h_{L,total}$, which can be presented as

$$h_{L,total}=h_{L,major}+h_{L,minor}=\sum_{i=1}f_i\frac{L_i}{D_i}\frac{v_i^2}{2g}+\sum_{j=1}K_{L,j}\frac{v_j^2}{2g} \tag{2.3.4}$$

where $h_{L,major}$ is the sum of pressure loss due to friction from the pipes, $h_{L,minor}$ is the sum of the pressure loss from components, $f_i$ is the friction coefficient, $L_i$ is the length of the pipe, $D_i$ is the diameter of the pipe and $K_{L,i}$ is the loss coefficient of the component. In this project, the friction factor is based on two different models, both depending on the Reynolds number, $Re$. The Reynolds number is a dimensionless quantity that gives the ratio between the inertial forces to viscous forces in the fluid. The flow regime mainly depends on this ratio, and is expressed for internal flow in a circular pipe as

$$Re=\frac{\rho v_{avg}D}{\mu} \tag{2.3.5}$$

where $v_{avg}$ is the average flow velocity (m/s) and $\mu$ is the dynamic viscosity of the fluid ($m^2/s$). The Reynolds number decides which model that is used to determine the friction factor. For $Re < 2300$, the flow is considered laminar, and the Darcy-Weisbach friction factor for fully developed laminar flow in a circular pipe is used

$$f=\frac{64}{Re} \tag{2.3.6}$$

For $Re > 2300$, the Blasius correlations for turbulent flow in smooth pipes are used,

$$f=0.316Re^{-0.25} \tag{2.3.7}$$

Moving on, the loss coefficients ($K_L$) of the different components is given by

$$K_{L,Exit}=\alpha \tag{2.3.8}$$

$$K_{L,BV}=0.05 \tag{2.3.9}$$

where $K_{L,Exit}$ and $K_{L,BV}$ is the loss coefficients for the pipe exit and fully open ball valve, respectiely, $\alpha \approx 1.05$ for fully developed, turbulent flow and $\alpha = 2$ for fully developed, laminar flow. Now Equation 2.3.3 will be altered to make an expression for the pressure outlet. By inserting Equation 2.3.4, setting $z_2 = h_{pump,u} = h_{turbine,e} = 0$, $\alpha_1 = \alpha_2$ and multiplying by $\rho g$ Equation 2.3.3 turns into

$$P_1=P_2-\rho g z_1+\alpha\frac{\rho}{2}\left(v_2^2-v_1^2\right)+\sum_{i=1}f_i\frac{L_i}{D_i}\frac{v_i^2}{2}\rho+\sum_{j=1}K_{L,j}\frac{v_j^2}{2}\rho \tag{2.3.10}$$

From the conservation of mass principle of incompressible, steady flow,

$$\dot{Q}_1 = \dot{Q}_2 \rightarrow v_1 A_1 = v_2 A_2 \tag{2.3.11}$$

where $\dot{Q}_1$ and $\dot{Q}_2$ are the volume flow rates at point 1 and 2, respectively, and $A_1$ and $A_2$ are the areas at point 1 and 2, respectively. This is an important relation which will be needed to determine the velocity at point 2 (or another arbitrary point) in the system,

$$v_2 = \frac{v_1 A_1}{A_2} = \frac{\dot{Q}_1}{A_2} \tag{2.3.12}$$

This concludes section 2.3. [5]

## 2.4 Convervation Laws and Volume Fraction Transport Equation

Before continuing to the CFD-analysis, it is important to see the equations behind the software. First, the basic principles of consersation of mass, momentum and energy needs to be applied. The derived equations are needed to solve the partial differential equation (PDE) system, and the continuity equation is given as

$$\frac{d\rho}{dt} + \rho \frac{\partial v}{\partial x} = 0 \tag{2.4.1}$$

where $\partial\rho/dt$ is the differencial of density with respect to time and $\partial v/\partial x$ is the partial differencial of velocity with respect to displacement (x-direction). The momentum equation, often referred to as the Navier-Stokes equations (usually shown for three dimensions), is

$$\frac{dv}{dt} + \frac{1}{\rho}\frac{\partial P}{\partial x} + f_D = 0 \tag{2.4.2}$$

where $\partial P/\partial x$ is the partial differencial of pressure with respect to displacement and $f_D$ is the drag force per unit mass. The energy equation is

$$\frac{dh}{dt} - \frac{1}{\rho}\frac{\partial \rho}{\partial t} - I_L = 0 \tag{2.4.3}$$

Here $dh/dt$ is enthalpy with respect to time and $I_L$ are losses per unit mass. These equations are simplified explanations of the conservation laws, and represents one dimensional, transient, single-phase fluid flow in a single pipeline segment without diffusion. [1] In addition to these equations, the volume of fluid (VOF) (or volume fraction) transport equation is applied in these simulations. The volume of fluid model is used to predict the distribution and the movement of the interface of immiscible phases. The volume fraction transport equation follows from the distribution of phase $i$ driven by the phase mass conservation equation:

$$\frac{\partial}{\partial t}\int_V a_i dV + \oint_A a_i \, v \cdot da = \int_V \left( S_{a_i} - \frac{a_i}{\rho_i}\frac{D\rho_i}{Dt} \right) dV - \int_V \frac{1}{\rho_i} \nabla \cdot \left( a_i \rho_i v_{d,i} \right) dV \tag{2.4.4}$$

Here $\boldsymbol{a}$ is the surface area vector, $\boldsymbol{v}$ is the mixture (mass-averaged) velocity, $\boldsymbol{v}_{d,l}$ is the diffusion velocity, $S_{ai}$ is a user-defined source term of phase $i$, and $D\rho_i/Dt$ is the material or Lagrangian derivative of the phase densities $\rho_i$. [6]

# 3. CFD-Analysis

In this segment the different aspects of the software used is presented. STAR-CCM+ is a powerful tool for simulating fluid dynamics, and a major part of the work done in this project is related to searching for information, trying and failing. In this chapter, the different stages of the CFD-analysis will be explained and justified.

## 3.1 Geometry, Regions and Boundaries

The geometry is based on 15 degrees of the actual accumulator shown to the left in Figure 3.1. It is reduced to decrease the number of faces in the mesh, and it will reduce the computational effort required to run the simulations. This allows for a larger timestep and will reduce the overall runtime. After creating the geometry, the parts of the geometry are assigned to two regions; Background and Overset.

In the Background region it is 3 different boundary types; Pressure Outlet, Wall and Symmetry Plane. The Pressure Outlet type is used at the outlet of the accumulator, and it is used to specify the pressure across the outlet. A field function, based on equation 2.3.10, is used to express this pressure. The Wall type is used to represent the walls of the accumulator, and the Shear Stress Specification is set to No-Slip. This means that the relative velocity of the fluid is zero at the wall, and this is normal when modelling viscous flows. The thermal specification for the walls is set to convection, which means that there will be a heat transfer in the form of natural convection (due to temperature differences) between the gas/fluid and the walls. The heat transfer coefficient is set to 5 $W/m^2K$. The Symmetry Plane type is needed for the walls of the geometry that is there because the model is reduced. It represents an imaginary plane that will not affect the fluid flow like ordinary walls.

The Overset also contains 3 boundary types. In the same manner as in the background, Wall and Symmetry Plane is used. In this region, the Overset Mesh type is used for the planes between the Overset and Background. These regions are coupled to create an interface between them, and this interface is used to create an overset mesh. This is explained in section 3.3. [6]

## 3.2 Physics Models

A physics continuum must be created and assigned to regions before the Overset and Background regions can be coupled. Physics models needs to be activated to simulate the physics of the problem. For the sake of order, the different models with explanations are listed in Table 3.1.

## 3.3 Overset Mesh

For the meshing of the model, an Overset Mesh was constructed. The principle of this method is to create an overlapping mesh around the moving body (piston). The background region encloses the entire accumulator, while the overset region is the smaller regions around the piston. Overlapping meshes are useful when dealing with moving bodies.

When creating an Overset Mesh, it is important to make sure there is at least 4-5 cells between the wall and overset boundary in the overset region. This is to ensure successful coupling between the background mesh and overset mesh as the piston moves. The basesize is set as 0.00466 metres in the mesh configuration, which is one-tenth of the overset height. This leads to approximately 10 cells between the wall and overset boundary. In Figure 3.1, a close-up on the overset mesh validates this.

When configurating the mesh, it is important to select the fitting meshers for the given situation. A corrupt mesh might lead to instability, poor results and cause the model to crash. In this model the Automated Mesh option is chosen, and the Surface Remesher, Trimmed Cell Mesher and Automatic Surface Repair meshers is added. The same order of magnitude of grid density is used in the overlapping region of the Overset and Background meshes. This minimizes the errors in the interpolating variables

| Model Selection for Fluid Continua | |
|---|---|
| Eulerian Multiphase | For defining the different phase materials |
| Exact Wall Distance | Allows computing the wall distance for the relevant turbulence and wall treatment models |
| Gradients | Select the gradient and limiter methods |
| Gravity | Enables gravity forces |
| Implicit Unsteady | For transient simulations |
| K-Epsilon Turbulence | Allows computing the turbulent kinetic energy and the turbulent dissipation rate to provide closure to the Reynolds-Averaged Navier-Stokes equations |
| Multiphase Equation of State | Physics model for multiphase simulations |
| Multiphase Interaction | For the interaction between phases |
| Realizable K-Epsilon Two-Layer | Combines the Realizable K-Epsilon model with the two-layer approach. |
| Reynolds-Averaged Navier-Stokes (RANS) | Utilizes the RANS equations |
| Segregated Flow | Models the flow |
| Segregated Multiphase Temperature | Possible to control thermal effects |
| Three Dimensional | For three dimensional problems |
| Turbulent | Sets viscous regime to turbulent |
| Two-Layer All y+ Wall Treatment | Model for modelling the RANS turbulence in the continuous phase |
| Volume of Fluid (VOF) | Simulate flows of two or more immiscible fluids on numerical grids capable of resolving the interface between the phases of the mixture |

Table 3-1: Model selection for the fluid continua [6]

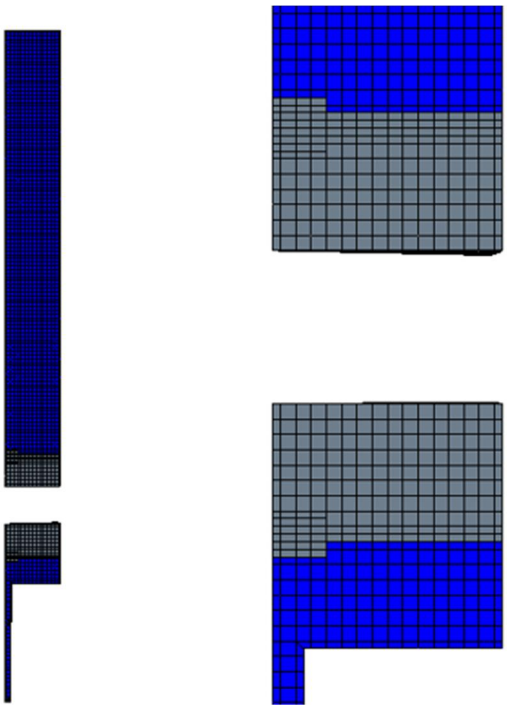

Figure 3-1: Mesh visualisation. Left: Entire model. Right: Close-up on Overset Mesh (grey)

between the two meshes. Surface Remesher is used to retriangulate the surface, which should improve overall quality of an existing surface and optimize it for the volume mesh models. The trimmed cell mesher is a method that produces a high-quality grid for mesh generation problems. Automatic Surface Repair helps correcting geometry problems that might occur. Surface Growth Rate is set to 1.3. [6]

## 3.4 Eulerian Phases

The gas and fluid in the simulation needs be defined as separate Eulerian phases. The Eulerian phases is created in the physics continua, and here the behaviour and material properties are chosen. For the nitrogen gas, the Energy, Exact Wall Distance, Gas, Ideal Gas and Turbulent models are applied. In the Gas model, the material properties are set. For nitrogen, the default settings are used since it is included in the material database available in STAR-CCM+. Models chosen for the barrier fluid is Energy, Exact Wall Distance, Liquid, Turbulent and User Defined EOS. For the fluid (Morlina S2 BL 5), there is no default option. The values for density, dynamic viscosity, thermal conductivity and so on needs to be set manually.

## 3.5 DFBI Motion and 6-DOF Body

To simulate the piston movement, a DFBI (dynamic fluid body interaction) motion object is created and assigned to the fluid region. A new DFBI Rotation and Translation needs to be created in the Motions node in the Tools section. This motion is assigned to the Motion Specification option in the Overset region. Afterwards, the different conditions for the DFBI-body is determined in the 6-DOF Bodies node under the DFBI section. The mass of the piston is set as one-twentyfourth part of the actual mass. Release time and ramp time is set based on the timestep and number of timesteps per iteration in the simulation. The Body Motion Option is specified as free motion in the z-direction, which means that the piston body can only move in the z-direction. A damping force and friction force are applied in the External Forces and Moments node. Forces and moments due to fluid flow and gravity force is also enabled for the piston.

## 3.6 Initial Conditions and Boundary Conditions

Field functions are used to define the initial conditions for the model. The initial pressure and temperature are different between the gas and fluid. Field functions are used to set the values above the piston to the initial values of nitrogen, and vice versa. A function is also needed to assign the phases (gas and liquid) to the regions they should be. These functions are applied to the initial conditions of the physics continua. As mention in Section 3.1, the pressure across the outlet is determined by a field function based on Equation 2.3.10. This is a boundary condition for the pressure outlet in the Background region.

## 3.7 Solvers

Solvers compute the solution during simulations. They can assemble the system of equations, solve the system of equations and provide source terms to equations that are solved by other solvers. The Implicit Unsteady solver controls the update at each physical time for the calculation, and here the time-step size is chosen. In the 6-DOF Solver the maximum number of iterations within a time-step is determined. To solve for the fluid flow, the Segregated Flow solver is used, which is recommended for incompressible flow at low Mach numbers. To control the solution of the turbulence transport equations in continuas for which a K-Epsilon model is activated, the K-Epsilon Turbulence solver is applied. The K-Epsilon Turbulent Viscosity solver controls the update of the turbulent viscosity, and in this solver the maximum ratio can help prevent unphysically high values of turbulent viscosity. The Segregated VOF solver solves the volume fraction conservation equation discussed in Section 2.4. Other solvers used is 6-DOF Motion, Load Balancing, Partitioning, Wall Distance and Segregated Energy. [6]

# 4. Results and Discussion

In this section the results from the simulations will be shown and reviewed. First off there will be a focus on the fluid pressure at 5 different precharge pressures in a chronological order; 40, 40.5, 41, 42 and 42.5 bara. Then the results from the different scenarios will be compared and discussed. Afterwards the temperature changes in the gas will be investigated. Furthermore, the velocity and volume flow behaviour and its effect on the results will be evaluated. At the end the results will be compared to measurements, and possible sources of error will be discussed.

## 4.1 Altering Precharge Pressure

Before going through the results in this section, it should be noted that the initial placement of the piston and temperature in the nitrogen gas is different for the different precharge pressures. The piston will be located lower, and the temperature will be higher for higher precharge pressures. For this reason, the calculated values for the initial piston position and nitrogen temperature will be shortly reviewed in this first section.

### 4.1.1 Overview of Initial Conditions

In the same manner as in Section 2.2, the temperature of the gas and the initial placement of the piston (taken as the height from the top of the accumulator down to the top of the piston) is calculated for different precharge pressures. These results are shown in Table 4.1.

| Precharge [bara] | 40 | 40.5 | 41 | 42 | 42.5 |
|---|---|---|---|---|---|
| Gas Temperature [K] | 310.6 | 313.4 | 316.15 | 321.6 | 324.4 |
| Initial Placement of Piston [m] | 0.5813 | 0.5865 | 0.5917 | 0.6020 | 0.6071 |

Table 4-1: Values for initial conditions at different precharge pressures. Note that the placement is given as the height from the top of the accumulator to the top of the piston.

### 4.1.2 Precharge Pressure 40 bara

In this simulation, the precharge pressure is 40 bara, the initial temperature of the gas is 310.6 K and the initial placement of the piston is at its highest compared to the other simulations. The pressure experiences a few increases after 6, 12, 22 and 27 seconds (Figure 4.1). This indicates an unstable movement of the piston, which is a result of less gas in the accumulator at lower precharge pressure. The decline is larger for the first 20 seconds, before it flats out and slowly decrease. This happens at about 44.9 bara. The points where the pressure increases are in the range of 0.01-0.02 bar and seems to be partly periodical (6-10 seconds between them). The discharge time is 42 seconds, and at this point the pressure is 44.15 bara.

### 4.1.3 Precharge Pressure 40.5 bara

In the second simulation, the precharge pressure is 40.5 bara, the initial temperature of the gas is 313.4 K and the initial placement of the piston is 5 mm lower than for the previous section. It seems like the pressure is experiencing slightly smaller pressure jumps in this simulation, besides for the one after 12 seconds (Figure 4.2). This indicates an unstable movement of the piston is reduced because of the increased amount of gas in the accumulator. Decline is larger for the first 12 seconds, before it flats out

and slowly decrease. This happens at about 45.2 bara. When comparing the differences between the simulations, it is important to notice that the discharge time is reduced for higher precharge pressures. In this simulation, the discharge time is 32 seconds at which the pressure is 44.2 bara.

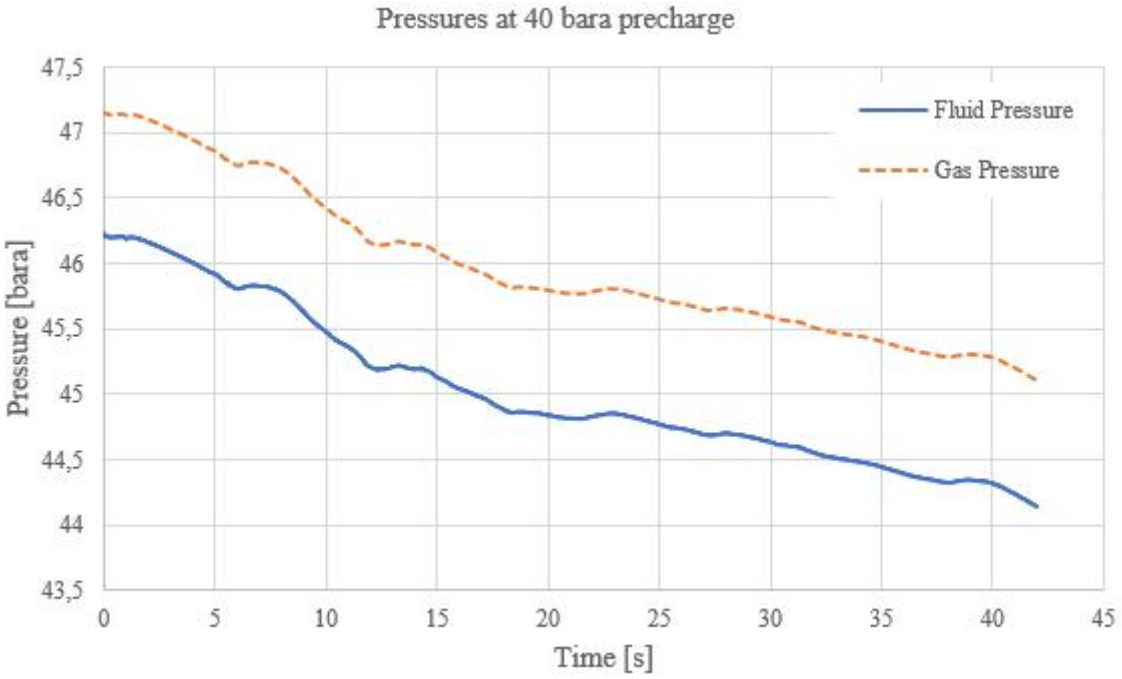


Figure 4-1: Pressure behaviour at 40 bara precharge

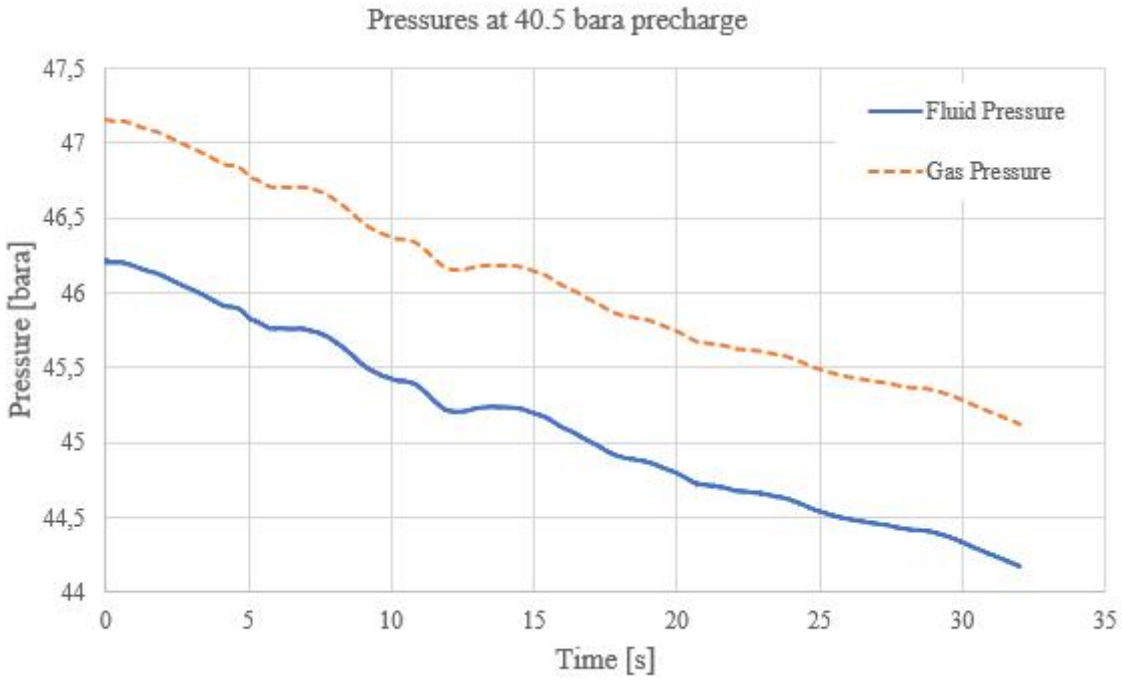


Figure 4-2: Pressure behaviour at 40.5 bara precharge

### 4.1.4 Precharge Pressure 41 bara

Here the precharge pressure is 41 bara, the initial temperature of the gas is 316.15 K and the initial placement of the piston has again dropped by 5 mm. The pressure has two significant jumps after 5 and 12 seconds (Figure 4.3). However, the pressure curve is smoother than for the previous two simulations. Discharge time is 30 seconds and the pressure is 44.4 bara at this point.

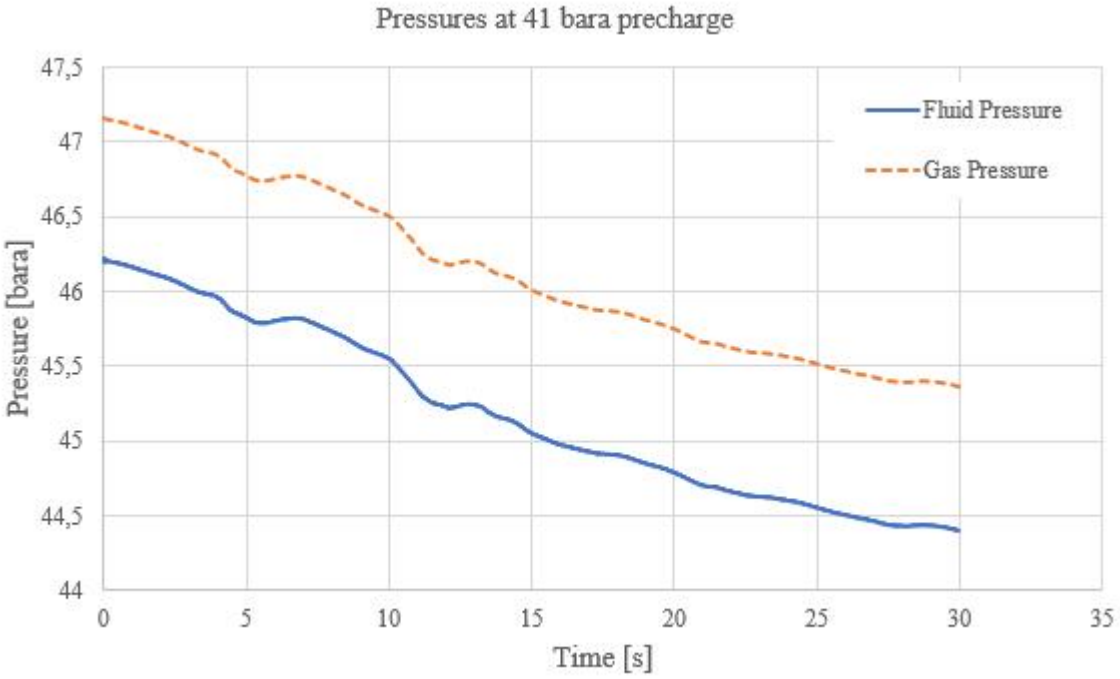


Figure 4-3: Pressure behaviour at 41 bara precharge

### 4.1.5 Precharge Pressure 42 bara

For a precharge pressure at 42 bara, the initial temperature of the gas is 321.6 K and the initial placement of the piston has dropped by 10 mm. Here, the pressure does not have any pressure jumps of significance. (Figure 4.4). After 2, 8 and 11 seconds it is relatively constant for approximately 0.5 seconds. This indicates that the pressure jumps from the previous simulations is even out at 42 bara precharge. Discharge time is 19 seconds at which the pressure is 44.6 bara.

### 4.1.6 Precharge Pressure 42.5 bara

For the largest precharge pressure of 42.5 bara, the initial temperature of the gas is 324.4 K and the initial placement of the piston is reduced by another 5 mm. The pressure displays the same constant behaviour at certain points similarly to the previous simulation (Figure 4.5). Discharge time is 20 seconds and the pressure is 44.8 bara at this point. The reason for the unexpected increased discharge time (compared to 42 bara precharge) is the result of some unnatural piston behaviour, and the discharge time is believed to be lower than this.

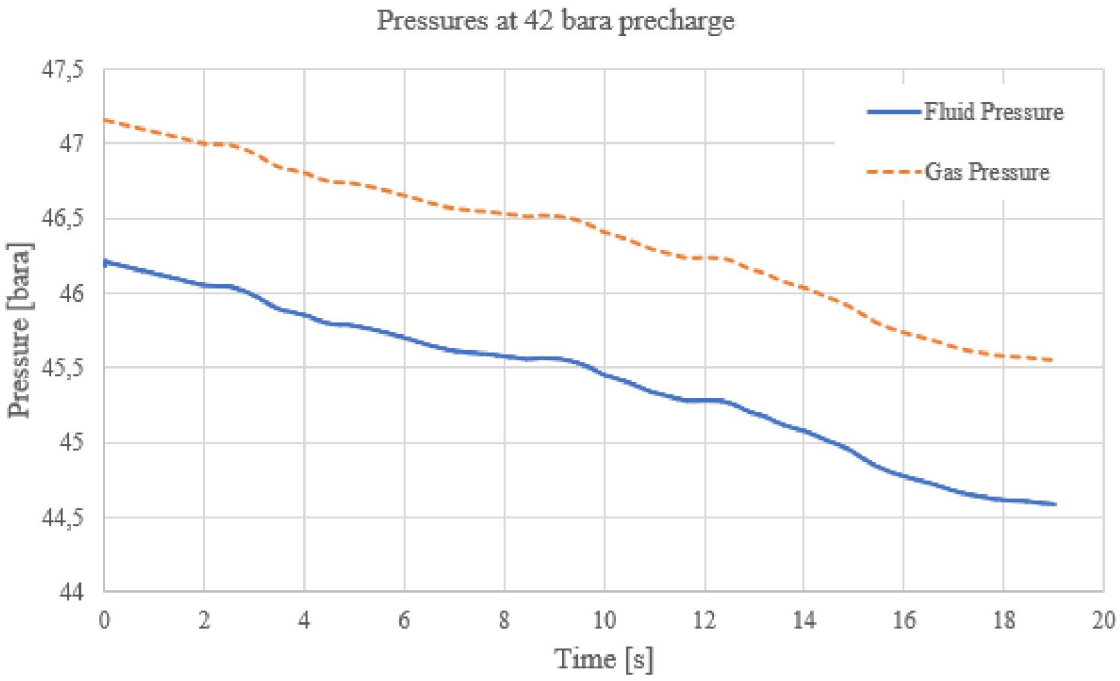


Figure 4-4: Pressure behaviour at 42 bara precharge

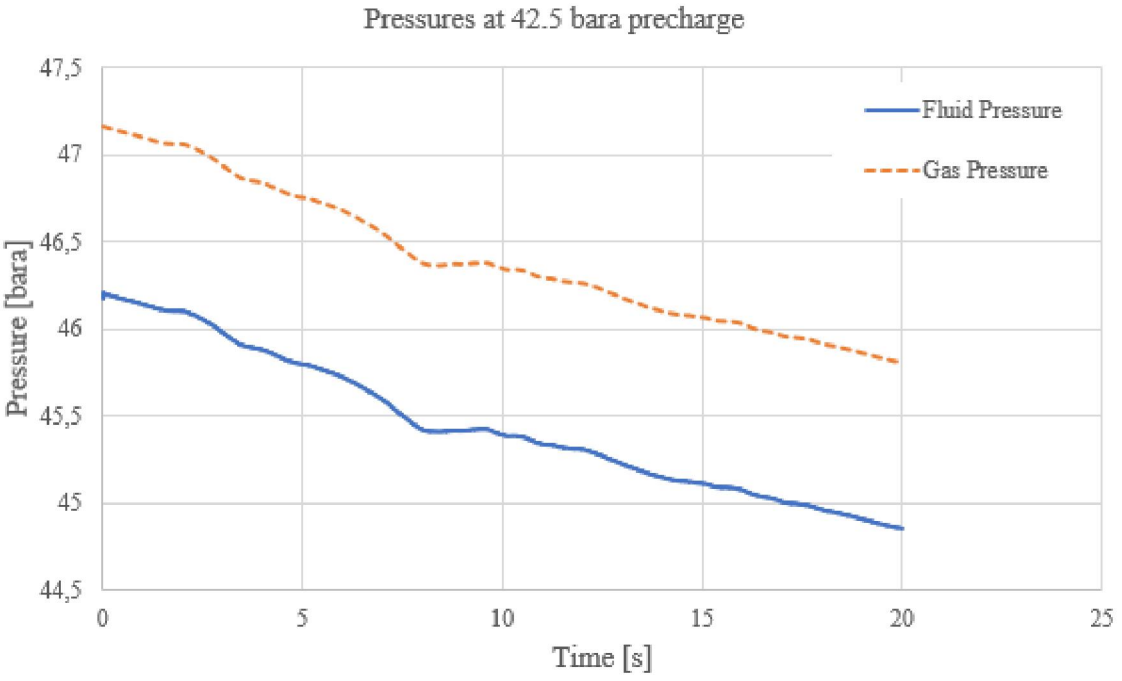


Figure 4-5: Pressure behaviour at 42.5 bara precharge

### 4.1.7 Comparison

The graphs of the fluid pressures from the different precharge pressures is illustrated together in Figure 4.6. This graph displays that the discharge cycle takes more time at lower precharge pressures. For the first 20 seconds, the graphs of the 40, 40.5 and 41 bara precharge behaves in a similar way. They experience pressure jumps at approximately the same time, but not of the same magnitude. However, after 20 seconds the 40-bara-graph makes a jump and then adapts to a smaller slope than the other two. The 40.5 and 41 bara graphs also obtain a smaller slope, but they differ from the smallest precharge.

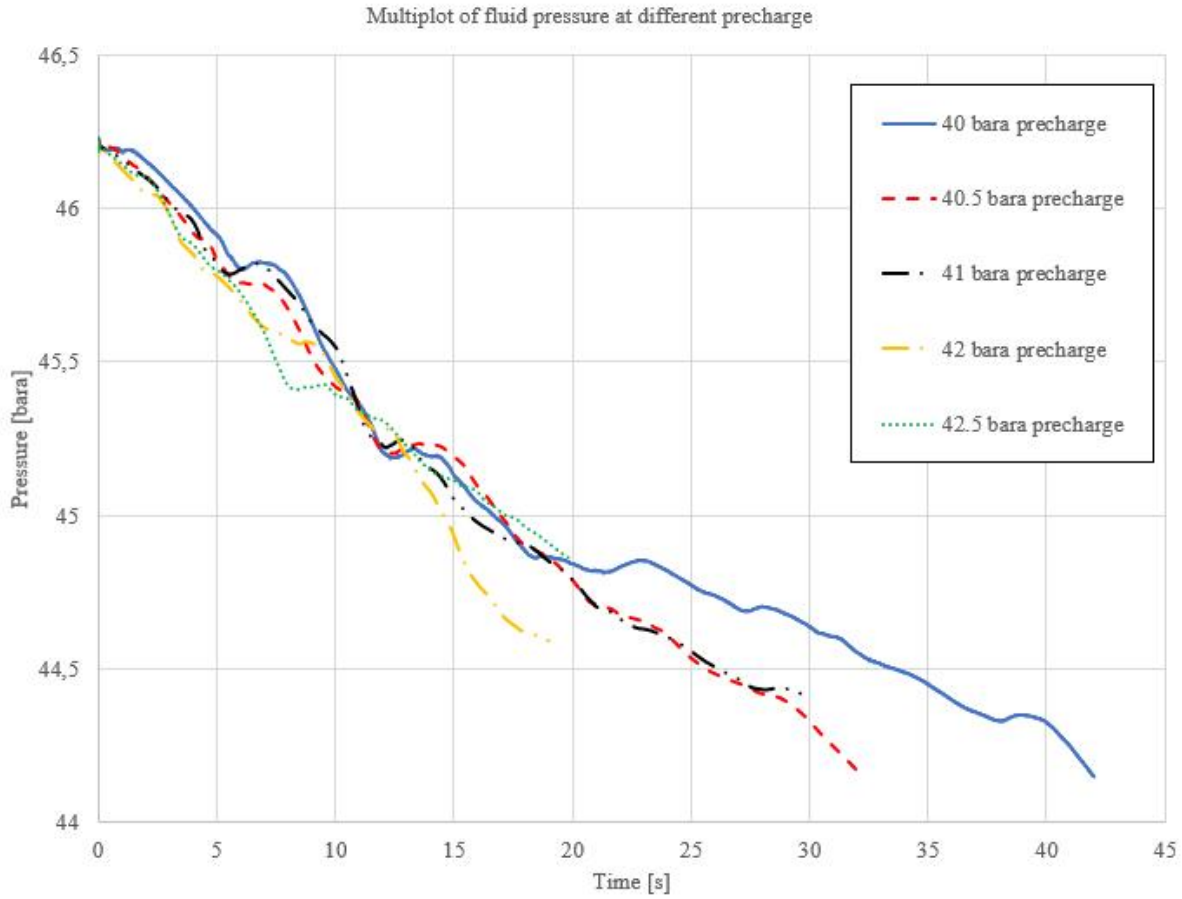


Figure 4-6: Fluid pressure at different precharge pressures

In Figure 4.7, the slopes of the different pressures for the whole simulation are shown. As expected, the slope at 40 bara precharge is the smallest one. At the lowest precharge, the accumulator contains the largest amount of barrier fluid when fully charged. This combined by the fact that the pressure drop is not much more than for the other simulations, it is reasonable to believe that this is valid. It also has the largest pressure jumps during discharge – contributing to a smaller slope. The slope at 40.5 and 41 precharge is almost identical. It is strange that the difference between 40 and 40.5 bara is that much larger than the difference between 40.5 and 41 bara, considering that the difference in precharge pressure is 0.5 bara in both situations. From Table 4.1 the numerical values for the slopes is listed. At 42 bara precharge the pressure is decreasing the most, which is a little surprising. One would expect the pressure drop to be fastest at the highest precharge pressure, but as mentioned in the previous section, the results from the last simulation should be viewed with caution.

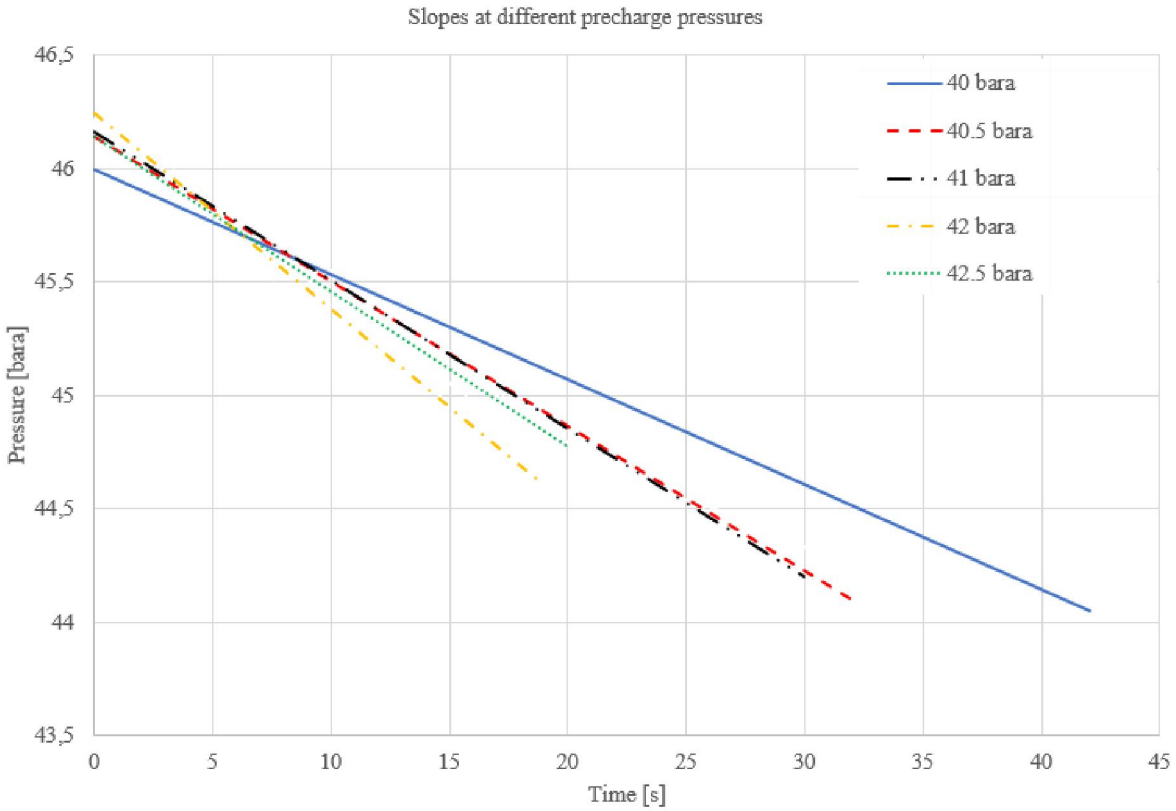


Figure 4-7: Slopes at different precharge pressures

| Precharge [bara] | 40 | 40.5 | 41 | 42 | 42.5 |
|---|---|---|---|---|---|
| Slope [bara/s] | -0.0463 | -0.0636 | -0.0653 | -0.0866 | -0.0682 |

Table 4-2: Numerical values of slopes

## 4.2 Temperature

In Figure 4.8, the temperature change in the nitrogen is displayed for the different simulations. In all simulations the temperature drops by approximately 0.1 K per second. This indicates that the gas lose heat to the surroundings because of the temperature difference. Similar to the pressure, it experiences a slight increase at the moments where the pressure increases. This is expected, since the temperature and pressure are dependant on eachother according to the ideal gas law. Another contribution to the temperature loss is the natural convection through the walls of the accumulator. As mentioned in the CFD-analysis, the heat transfer coefficient is set to 5 $W/m^2K$, and the ambient temperature is set to 300 K. This contribution is relatively small. The decrease in gas temperature will lead to less kinetic energy in the gas, which again leads to less collisions between the molecules. The more collisions, the more resistance against fluid flow. Therefore, the viscosity of the nitrogen decreases during discharge.

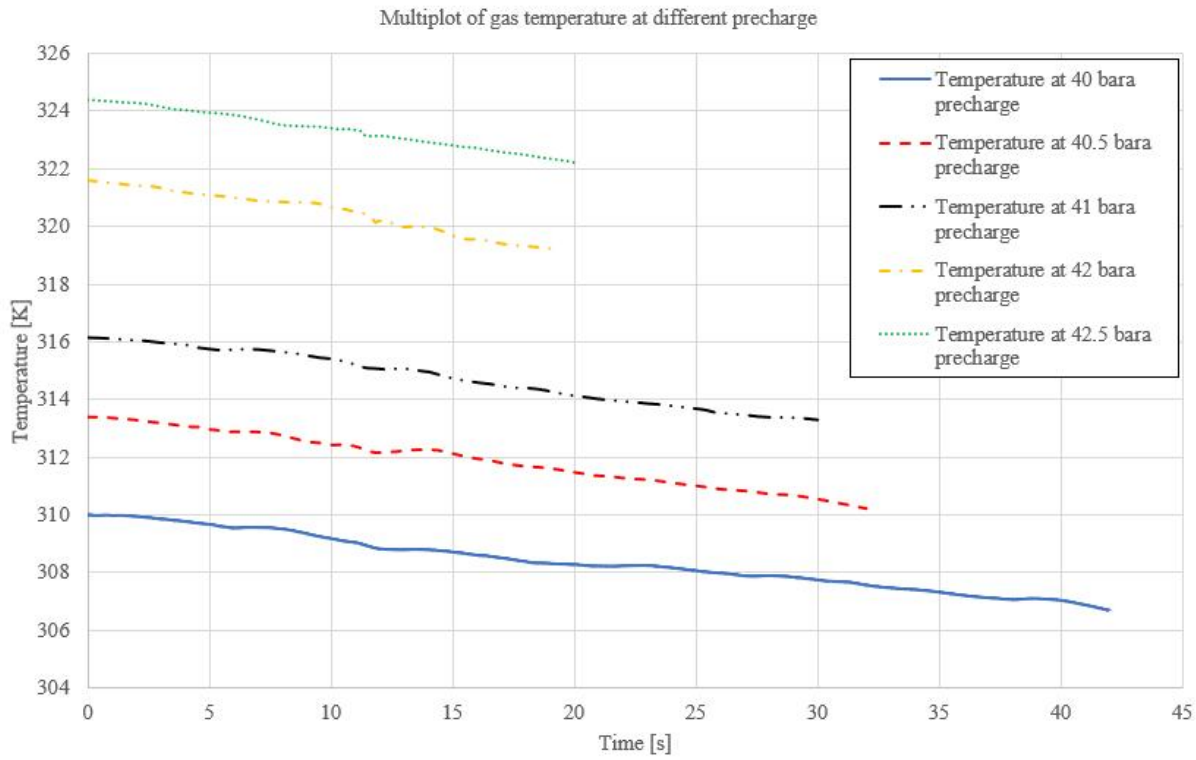


Figure 4-8: Gas temperature behaviour at different precharge pressures

## 4.3 Volume Flow, Velocity and Comparison with Measurements

From the measurements made by the flow meter, the average volume flow is approximately 0.5 litres per hour during discharge. This means that the fluid leaving the accumulator must leave the accumulator at approximately 0.9E-3 m/s. In the model, the velocity starts at 0.095 m/s and slowly reduces to 0.04-0.06 m/s in all simulations (Figure 4.10). This corresponds to a volume flow ranging from 25 to 50 litres/h (Figure 4.9). Large volume flow is the main reason for the unrealisticly fast discharge. It should have taken more time. But it proved difficult to achieve a small enough velocity and this results in the large volume flow. However, it is still possible to analyze the results and draw conclusions.

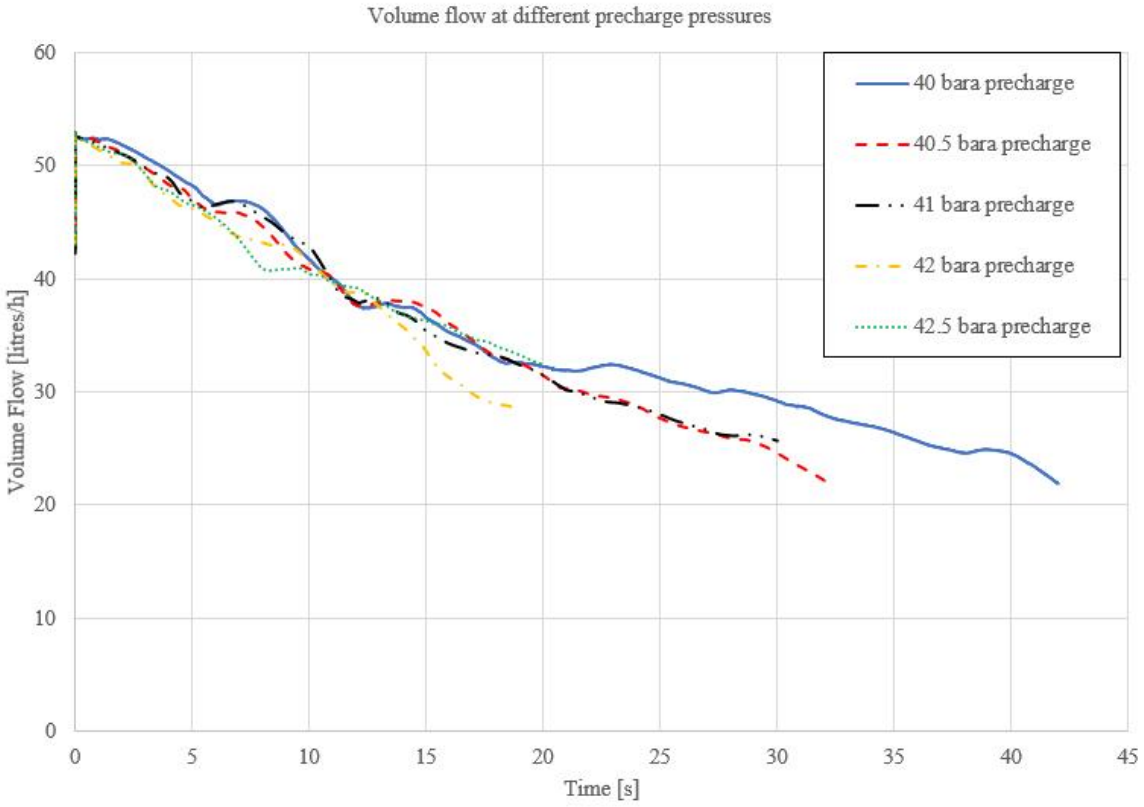


Figure 4-9: Volume flow at different precharge pressures

According to the measurements from the real installation, there are noe pressure jumps during discharge. However, the pressure is registered at a limited amount of times. It has 35 registrations over 156 seconds. In Figure 4.11, instead of flating out at the expected minimum pressure (44.2 bara) the pressure keeps decreasing. However, at this point, the piston stops moving. It seems like the model recognizes this to be the minimum pressure somehow (since the piston stops moving), but without the pressure ceasing to drop. The pressure behaviour beyond this point (where the piston stops moving) is considered unphysical and is therefore disregarded in this report and is not included in the graphs.

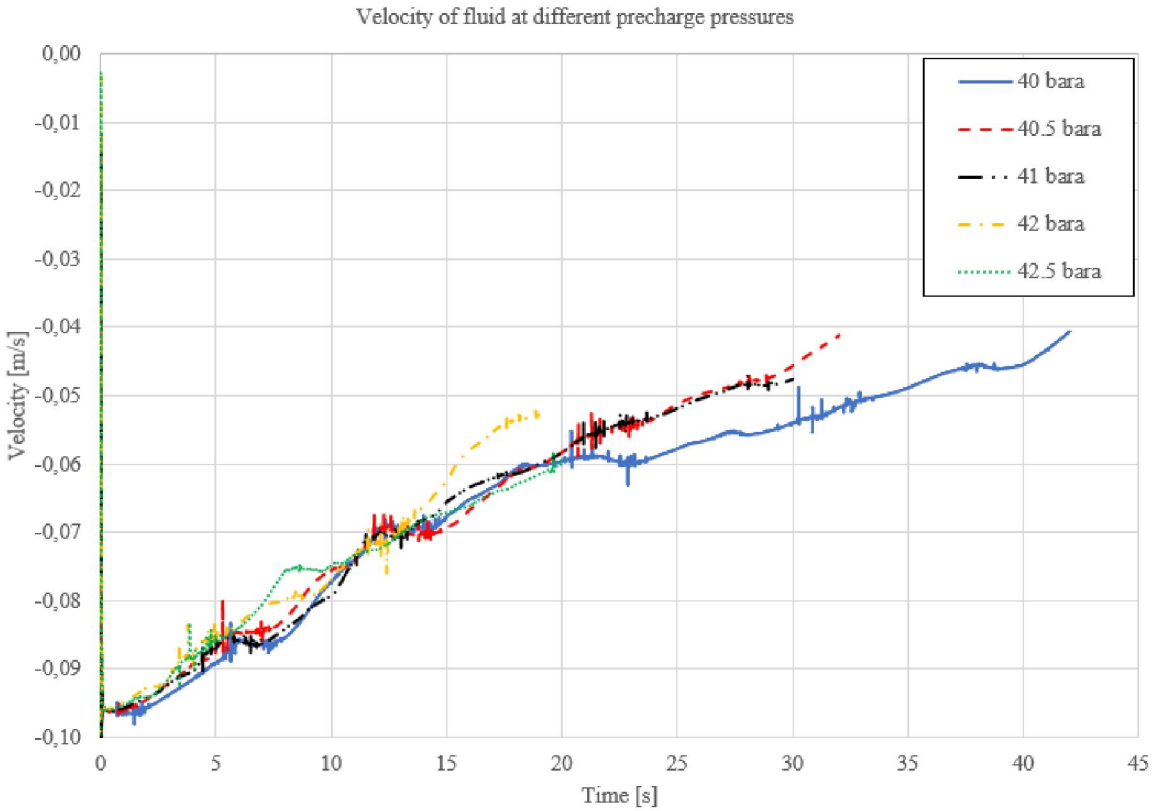


Figure 4-10: Fluid velocity out of accumulator

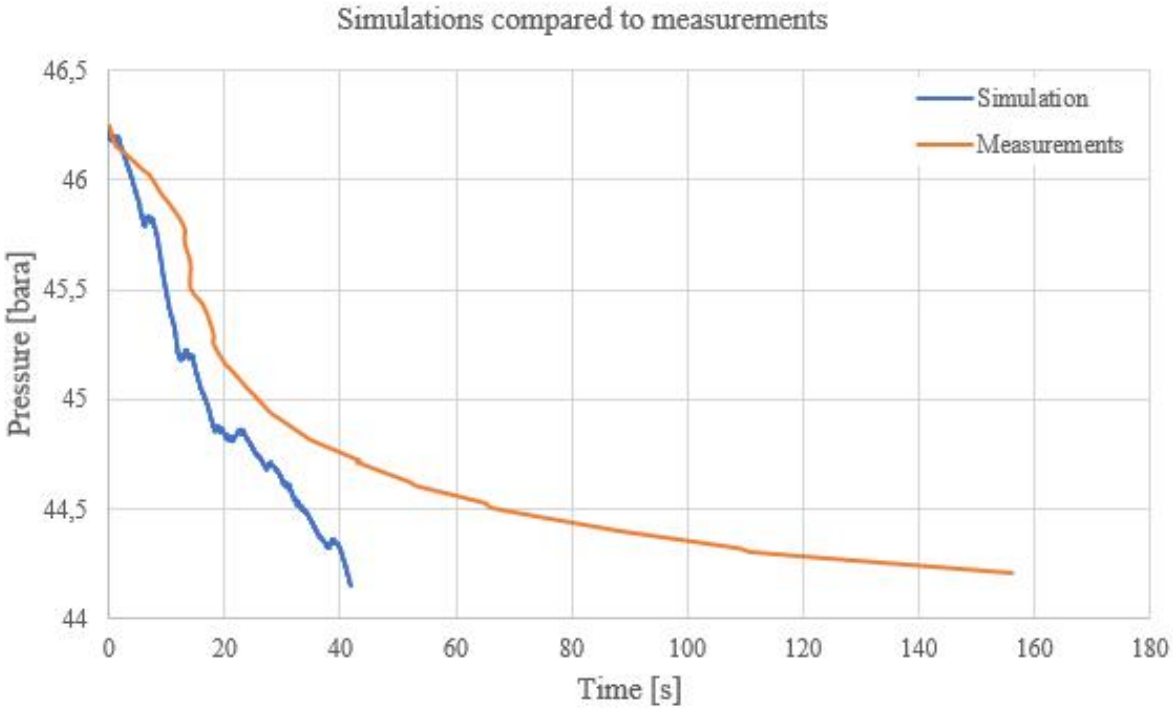


Figure 4-11: Simulation values compared to measurements for 40 bara precharge

# 5. Conclusion

According to the results, discharge time is affected by altering the precharge pressure. The accumulator discharges faster for higher precharge pressures. This is because higher precharge leads to less barrier fluid in the accumulator when fully charged (lower initial placement of piston), which means it has less fluid to discharge. From the graphs in the results, the pressure is more stable at higher precharge pressures. This is due to the increased amount of nitrogen in the accumulator when increasing precharge pressure. The driving force becomes larger, which stabilizes the piston motion.

The volume flow starts at approximately 50 l/h and drops to 25 l/h in all simulations. This is a large deviation from the measured average volume flow of 0.5 l/h, and this leads to a faster discharge time in the model. For the lowest precharge pressure simulated at 40 bara, which is the same value for the measured accumulator discharge, the discharge time is 42 s compared to 156 s for the actual accumulator. The results from this thesis should therefore be assessed with caution.

The temperature of the gas reduces by approximately 0.1 K/s in all simulations. It does not display any interesting behaviour, but it should be noted that the temperature increase with larger precharge pressure. This increase in temperature means that the gas loses more heat to the surroundings, and this will lead to a faster pressure drop for higher temperature.

### Future Work:

For future projects, it would be interesting to:

- Simulate a full-size version of the accumulator during discharge, since symmetry conditions seemed to result in instabilities and unknown factors that pollute the solution
- Correctly implement a solid region for the piston to analyse heat transfer through the piston
- Simulate a model that discharges according to the field data, where the volume flow is lower, and the pressure stabilizes around minimum pressure

# Bibliography

[1] G. Geiger, «*State-of-the-Art in Leak Detection and Localisation*», 2006.

[2] X.-J. Wang, M. F. Lambert, A. R. Simpson and J. P. Vitkovský, «*Leak Detection in Pipelines and Pipe Networks: A Review*», 2001.

[3] A. Kjølle, «*Oljehydraulikk*», 2nd. edition, Tapir, 2007.

[4] Y. A. Cengel and M. A. Boles, «Thermodynamics: An Engineering Approach», 8th edition, McGraw-Hill Education, 2015.

[5] Y. A. Cengel and J. Cimbala, «*Fluid Mechanics*», 3rd. edition, McGraw-Hill Education - Europe, 2013.

[6] Siemens, «*Simcenter STAR-CCM+ User Guide*» vol. 13.04, 2018.